Investigating the Porosity of Agarose Hydrogel through Single Fluorescent Particle Tracking via Confocal Microscopy

Abstract

Agarose hydrogel has become a quintessential polymer to the study of biological physical phenomena. While there are several techniques to study it on the scale of nanometers, expensive experimental setups limit further developments; our lack of understanding of its internal structure may impair further scientific research using agarose hydrogel. In this work, a recently developed technique applying a standard epifluorescence confocal microscope to single particle tracking along with a culminating laser scanner was used to determine the trajectory of quantum dots diffusing through agarose hydrogel in three-dimensional space. In particular, we utilized an extremum seeking algorithm that automatically moves towards the peak of the measured intensity within the point spread function and, by association, to the vicinity of the source particle. By plotting the paths of the diffusing quantum dots, which produced highly concentrated clusters where pores in the agarose were located, a visual representation of the structure of the hydrogel was produced. Our analysis of the hydrogel produced an estimate of the pore size and distribution for 2.6% agarose, as well as insight as to the valuable potential of applying single particle tracking via confocal microscopy to further scientific research of the porosity of hydrogels.

Introduction:

Often used to encapsulate drugs and simulate tissue, agarose hydrogel has undeniable utility and potential to many vital fields of science, including biomedical engineering and pharmaceuticals. Today, agarose hydrogel is a vital component of many new technologies, ranging from pharmacology to tissue engineering to food sciences to genetics [1]. For example, agarose hydrogel nanoparticles have been applied to novel injectable drug delivery systems that negate the need for emulsifiers that may change the effects of encapsulated protein and peptide drugs [2]. Its convenience, low cost, and safeness, makes it an ideal candidate for an injectable scaffold for implantation surgery [3] -- qualities that are made even more appreciable given that agarose hydrogel is extremely compatible with living tissue and can easily adhere to nearby cells, making for a minimally invasive surgery. Moreover, recent advances in tissue engineering show that agarose hydrogel is particularly well suited to fostering cell growth, due to its tissue-like nature and its controllability (in other words, adjusting hydrogel parameters such as the swelling ratio and network mesh size may be easily accomplished) [4]. It is clear that agarose hydrogel holds, and will continue to hold, its reputation as a valuable and promising component in future scientific endeavors.

Hydrogels consist of networks of cross-linked hydrophilic polymers that easily absorb and retain water without dissolving in it [5]. Agarose is a naturally occurring polysaccharide that can be extracted from seaweed, forming the base for the natural hydrogel that we investigate in this research project. The internal structure of agarose hydrogel may be thought of as built with a large number of rigid polymer chains, arranged such that there may be larger gaps of empty spaces, which we call pores. The size, shape, and arrangement of these pores affect many

mechanical and chemical properties of the agarose; for example, the porosity of a hydrogel affects polymer:crosslinker ratio, swelling, and permeation [6, 7].

However, current scientific literature has only insufficiently characterized the porosity of agarose hydrogels. In particular, there is a clear lack of reliable and efficient methods to accomplish this task. Previous methods have included, amongst others, using scanning electron microscopes only on hydrogels that are over ninety-seven percent water (which involves technical difficulties that impede its efficiency) [6] and using atomic force microscopy to image the surface of the gel (which may warp the structure of the gel due to applied physical force and also lends itself to only two-dimensional analysis of the pore size) [8]. What is important to note is that the porosity of the hydrogel does not remain constant when its other mechanical factors are changed [6]. In other words, without a reliable method to measure the porosity of the gel, researchers have no way to separate the effects of the changing porosity from the effects of their treatment. Our lack of understanding of their internal structure therefore greatly undermines the accuracy of research that utilizes agarose hydrogel. A thorough investigation of the structure of agarose with a resolution on the scale of nanometers could have a significant impact on projects that utilize agarose hydrogels.

In our research project, we applied a recently developed microscopic technique in which confocal microscopy was applied to single particle tracking [9]. Using this method, we tracked the path of diffusing quantum dots as they traveled through the pores of a 3.6% concentration agarose hydrogel. After collecting the data, we then fitted the pores of the agarose to an ellipsoid and performed statistical analysis on the sizes and lengths of the pores. To our knowledge, the internal structure of agarose hydrogel has not yet been investigated through single particle tracking of quantum dots -- an effective technique that yields a pathway to investigate a

hydrogel's porosity through a three-dimensional perspective without affecting its internal structure.

In short, the main goals of this research project are (1) to develop a procedure to consistently measure and calculate the size and shape of pores, (2) to interpret the data collected by fitting it to an ellipsoid and calculating the distribution of pore sizes, and (3) to assess the viability of using single particle tracking through confocal microscopy.

Materials and Methods:

To investigate the structure of agarose, we tracked the path of particles traveling in the matrix of the hydrogel using an adaptation of confocal microscopy to particle tracking.

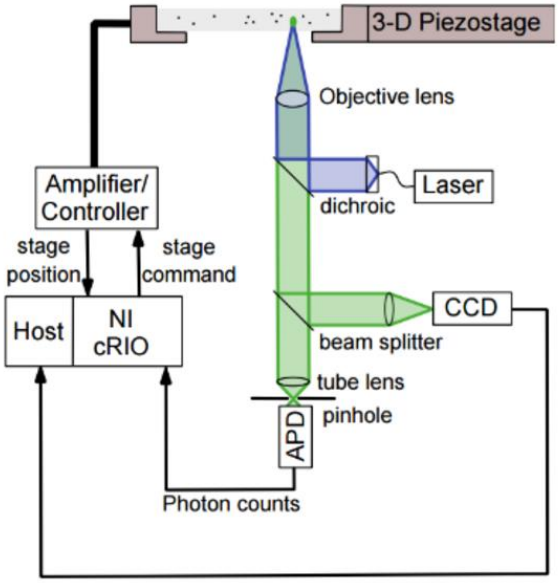

Figure 1[1]. A diagram of the set-up of the equipment used in our research. High-intensity fluorescent light from the laser is sent through a sample of quantum dots diffused through agarose, which emit protons in response. These protons travel through the dichroic mirror to the beam splitter, where 30% of the protons travel to the charge coupled device (CCD - the camera that displays an image on our computer screen) and 70% travel to the avalanche photodiode (APD), which measures the photon counts from each part of the sample. This information is used by the algorithm to track the particle.

[1] From "Tracking single fluorescent particles in three dimensions via extremum seeking," by T. Ashley et al. (2016) with permission (originally published in Biomedical Optics Express). Reproduced with the permission of the author(s).

Single Particle Tracking Algorithm

Ordinarily, confocal microscopy is applied to larger structures like cells; however, our method adapted it for single particle tracking by implementing an algorithm, which we helped develop, that adapted the confocal microscope to nanocrystals of radius 250 nm and less. This algorithm seeks the extremum of the pattern of light intensity, or point spread function, using an avalanche photodiode [9]. Because the particle is located at the peak of the intensity, by pursuing the point of maximum intensity, this algorithm can locate and track a single particle diffusing through a medium. The algorithm follows as such [9]:

$$\begin{aligned}
\dot{x}_s &= R\left(\omega_1 \sin\theta\cos\phi + \omega_2 \cos\theta\sin\phi\right), \\
\dot{y}_s &= -R\left(\omega_1 \sin\theta\sin\phi - \omega_2 \cos\theta\cos\phi\right), \\
\dot{z}_s &= \omega_1 R\cos\theta, \\
\dot{\theta} &= \omega_1\left(1 - K_p\frac{dI}{dt}\right), \quad \dot{\phi} = \omega_2,
\end{aligned}$$

In this algorithm, I is the intensity measurement at time t. The user may adjust R (the radial distance between the particle and the volume of sample that may be efficiently detected through the microscope), K_p (the rate of convergence to the sphere), and ω_1 and ω_2 (rates of oscillation of the focal volume) [9].

Sample Preparation Procedure

To create samples, 22CIR-2 coverslips were placed on a clean, dry lab table covered with a large delicate task wiper. A hydrophobic barrier pen was used to draw circles along the perimeter of the coverslips, which were then set aside to dry. 1 μL of quantum dots and 500 μL of water were centrifuged at 500 RPM to ensure proper mixture and to prevent clustering. To create one sample slide, 5.235 g of water and 0.186 g of agarose was combined in an Erlenmeyer flask and heated in a microwave until boiling, whereupon it formed a thick clear gel. Next,

5.772 g of glycerol was stirred into the solution. To prepare the slides, 1 μL of the prepared 1:500 quantum dot solution was pipetted onto the prepared 22CIR-2 coverslip; then, 20 μL of the agarose-glycerol mixture was then pipetted onto the slide and manually mixed into the quantum dots for 15 seconds. An 18CIR-2 coverslip was placed on top of the gel and sealed with a clear sealant, applied to the junction of the 18CIR-2 and 22CIR-2. The sample was then loosely covered with aluminum foil to prevent bleaching and cooled to room temperature. Next, the slides were further cooled in a refrigerator to slow down the movements of the quantum dots. When ready to be tested, the cooled slides were mounted on a holder, which was placed on the piezoelectric nanostage of the microscope.

Single quantum dots were first manually located, upon which our single particle tracking method was used to accurately predict and follow the trajectory of the path. The algorithm was implemented in LabVIEW on a National Instruments compact Reconfigurable Input Output (cRIO) system using a sample rate of 1 kHz. The acquired data was then analyzed in MATLAB, where we manually excised the data pertaining to randomly selected pores and fitted it to an ellipsoidal approximation.

We conducted this experiment largely independently; to be specific, we maintained and utilized the laboratory equipment, prepared samples, collected data, wrote any code necessary to our projects, and performed data analysis. Our mentor guided us throughout our research by suggesting ideas to improve our procedures or analyze our data. The undergraduate student occasionally assisted us with equipment malfunctions. The last contributor suggested various methods to analyze the data we collected that we eventually used in our project.

Results:

Statistical Analysis:

We were able to collect suitable data from 434 trials, each with anywhere from several to hundreds of pores. In order to randomly select the data to be analyzed, we used a random number generator to pick data files and to randomly select pores within that data file.

The average volume for the fifty-four analyzed pores was 4.3417×10^{-4} μm^3, with a standard deviation of 1.4558×10^{-4}. The smallest pore volume was 1×10^{-4} μm^3 and the largest was 7.52×10^{-4} μm^3. Whether or not the data follows a normal distribution is questionable; though the Q-Q plot (Figure 8) is fairly promising (most of the data adheres to the 45-degree reference line, except for the anomalies between quantiles -2 and -1.25), the shape of the data displayed on the histogram (Figure 7) leaves much to be desired.

We found that the average values of *a*, *b*, and *c* were, respectively, 6.0644×10^{-2} μm, 4.5848×10^{-2} μm, and 3.6340×10^{-2} μm (with standard deviations of 1.1745×10^{-2}, 6.6169×10^{-3}, and 6.1717×10^{-2}). The length of *a* ranged from 3.5443×10^{-2} μm to 9.0838×10^{-2} μm; b from 3.0806×10^{-2} μm to 6.0179×10^{-2} μm; and c from 2.1146×10^{-2} μm to 4.9046×10^{-2} μm. The distributions are displayed in Figures 9-11.

Tracking Run Optimization

The novelty of such an experiment lent its way to initial difficulties that we needed to overcome to obtain accurate results. Since the confocal microscopy setup involved refracting light into a pinhole the size of nanometers, the slightest movements in the setup process led to a misalignment of the APD and an inability to track the particle as it moved through the hydrogel. Shot noise also led to variability in the distribution of photons collected by the APD from various tracking runs. Utilizing intensity feedback from the point spread function, we were able to make

subtle changes to the horizontal and vertical components of the APD that would maximize the APD counts for optimized tracking runs.

Bleaching was another issue that resulted from our experimental setup. When the quantum dots bleached due to excessive exposure from the laser, or ambient light, both the CCD and APD would not detect photons, and thus the tracking algorithm could not follow the movement of the particle through the hydrogel. However, decreasing the power of the laser too low led to its own complications, as not enough photons were emitted from the fluorescent particle itself, leading to rather fragmented tracking runs. Through preliminary runs, we determined that the optimal power range for the laser is 500 mW and kept it constant throughout our tracking runs.

Though we used glycerol to slow the movement of the quantum dots (a viscosity of 1.412 Pa·s compared to water's 8.90 x 10^{-4} Pa·s), we found that at times, the particle still diffused too quickly through the hydrogel; therefore, we cooled the slides to slow the particles down. To mitigate the effects of clustering quantum dots that might impede results, we centrifuged quantum dot solutions for thirty seconds with 500 RPM. We also varied the concentration of the quantum dot solution in preliminary runs from 1:250 μL up to 1:1000 μL, and determined that the optimal quantum dot solution was 1:500 μL. To prepare data for analyzation, all data was collected under the assumption that 3 APD counts or lower would be disregarded as background noise, in a laboratory of 21°C with relative humidity of 55%, to ensure consistency of results.

Volume Approximation

The volume of individual pores was estimated by calculating the lengths of the semi-principal axis (a, b, c) of an ellipsoid given by $\frac{x^2}{a^2} + \frac{y^2}{b^2} + \frac{z^2}{c^2} = 1$. The values were then used to

estimate the volume of an ellipsoid using the equation $V = \frac{4}{3}\pi abc$. We created a principal component analysis function in MATLAB, which normalized the data to reorient the initial semi-principal axes of the data points to fit the largest possible variance.

The next step involved computing the covariance matrix as well as eigenvectors and corresponding eigenvalues. Using the eigenvalues of the covariance matrix of the normalized position data, the function created a new matrix of coordinates to adjust for the linear transformation. Next, we computed the eigenvalues and ranked the eigenvectors from highest to lowest by eigenvalues; these corresponded, respectively, to the new *a, b,* and *c* axes of the ellipsoid. Using the aforementioned ellipsoidal volume formula, we calculated an approximation of the pore volume. An eigenvector matrix was then constructed and the sample data was transformed into a new subspace through singular value decomposition given by $Y = W^T \cdot X$, where X is the original matrix [10]

Diffusion Coefficients

The unpredictable anisotropic movement in the directed motion of the fluorescent particle was represented by the diffusion coefficient between the particle and agarose through the Stokes-Einstein equation: $D = \frac{k_b T}{6\pi\eta r}$ [10].

The probability distributions for the diffusion coefficient D_x a result of a single particle tracking run, where $x_{p,k}$ represents the movement of the particle stochastically in discrete time according to probability density [9].

$$p_{V_x, D_x}(x_{p,k+1}|x_{p,k}) = \mathcal{N}[x_{p,k+1}]\left(x_{p,k} + V_x\Delta t, 2D_x\Delta t\right)$$

Here, $N[x](\mu, \sigma^2)$ represents a normal distribution, with mean μ and standard deviation σ^2 evaluated at x. Note that the *y* and *z*-axes are of identical form when calculating D_y and D_z. Differentiating, the maximum diffusion coefficient in a tracking run is

$$\hat{D}_{x,e+1} = \frac{1}{2N\Delta t} \sum_{k=1}^{N-1} \sum_{i=1}^{M} \sum_{j=1}^{M} w_{k|N,e}^{ij} \left(x_{k+1|N,e}^{j} - x_{k|N,e}^{i} - \hat{V}_{x,e+1} \Delta t \right)^2$$

From this equation, we found that the estimated diffusion coefficients for our tracking runs were (0.139, 0.082, 0.087) μm^2 per second for x, y, z respectively [9]. This was done by employing the SMC-EM algorithm, which utilized the expectation maximum (EM) and sequential Monte Carlo (SMC) method to localize the particle and infer diffusion coefficients [12]. Diffusion coefficients can further be used to determine the structure of agarose in mechanical flux applications, including the mobility and flexibility of various macromolecules within the gel [7].

Illustrations:

The Data Analysis Process

Figures 2 through 6 show examples of the raw data collected, and a visual step-by-step process of how we prepared our data from analysis, from its raw form to its completed analysis.

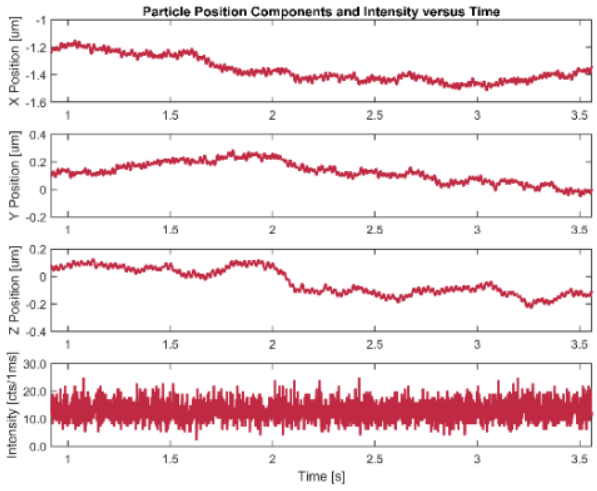

Figure 2. These four graphs display the x, y, and z components of the particle's trajectory against time, as well as a measure of the intensity of light. Note that the intensity of light, despite the variable "shot noise" dips and rises, is both consistent and high. This indicates that the algorithm has properly locked onto a particle and is consistently tracking it.

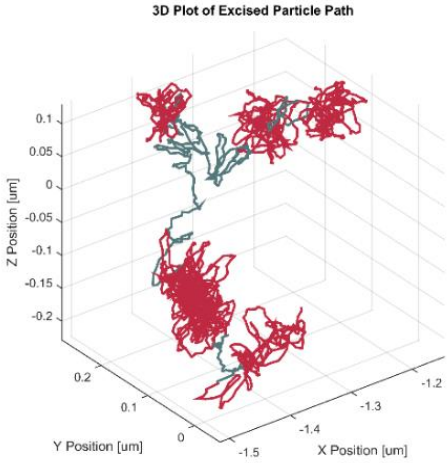

Figure 3. A portion of raw data. The line represents the path of a single quantum dot as it diffuses through the hydrogel. When the quantum dot reaches a pore, it will "ricochet" off of the pore's bounds until eventually finding an exit. Here, it is immediately obvious where the quantum dot has encountered a pore (colored red).

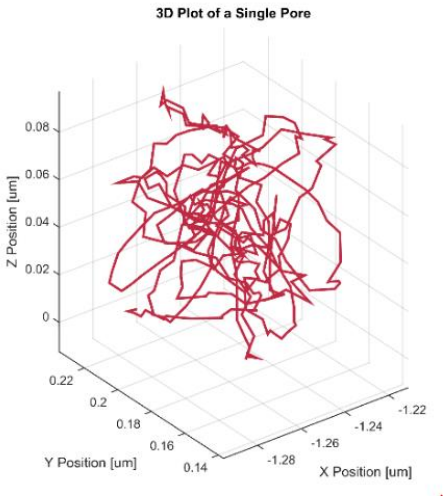

Figure 4. A plot of the single pore (colored red in Figure 3). Note the ellipsoidal shape, which we will approximate in our analysis.

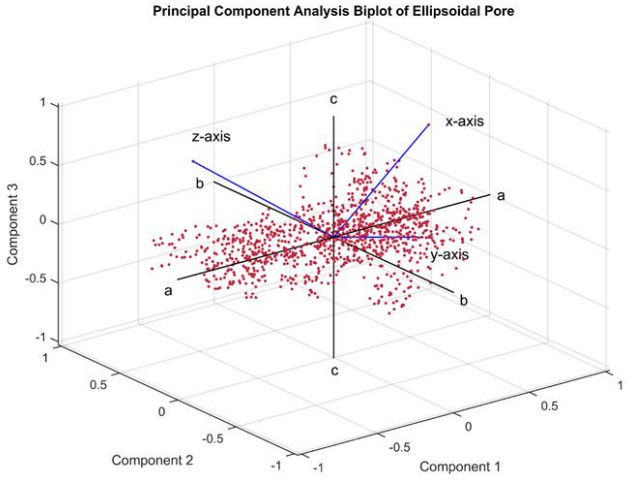

Figure 5. A PCA biplot of the same pore. Each dot represents the location of the particle at a given time. The original x, y, z-axes are shown in blue, and the new axis of the normalized principal component coefficients following PCA are shown in black. The orthogonal semi-principal axis of the ellipsoidal fit coincide with the eigenvectors and maximum variances of the data.

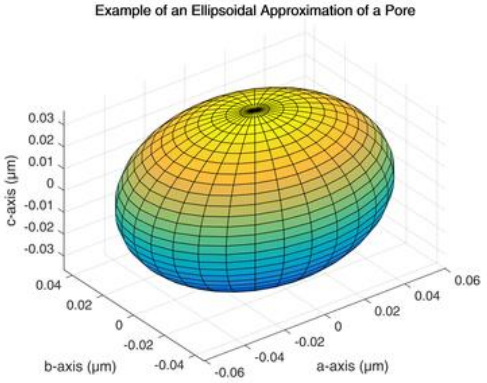

Figure 6. A visual representation of the average pore size we calculated.

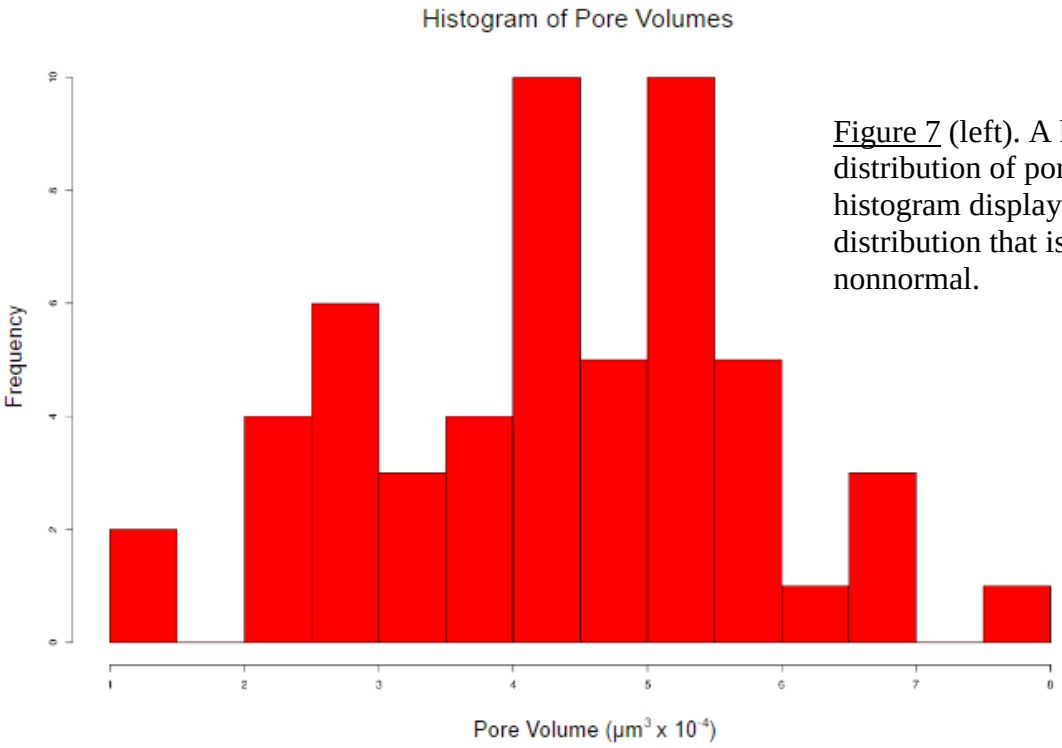

Figure 7 (left). A histogram of the distribution of pore volumes. The histogram displays an irregular distribution that is distinctly nonnormal.

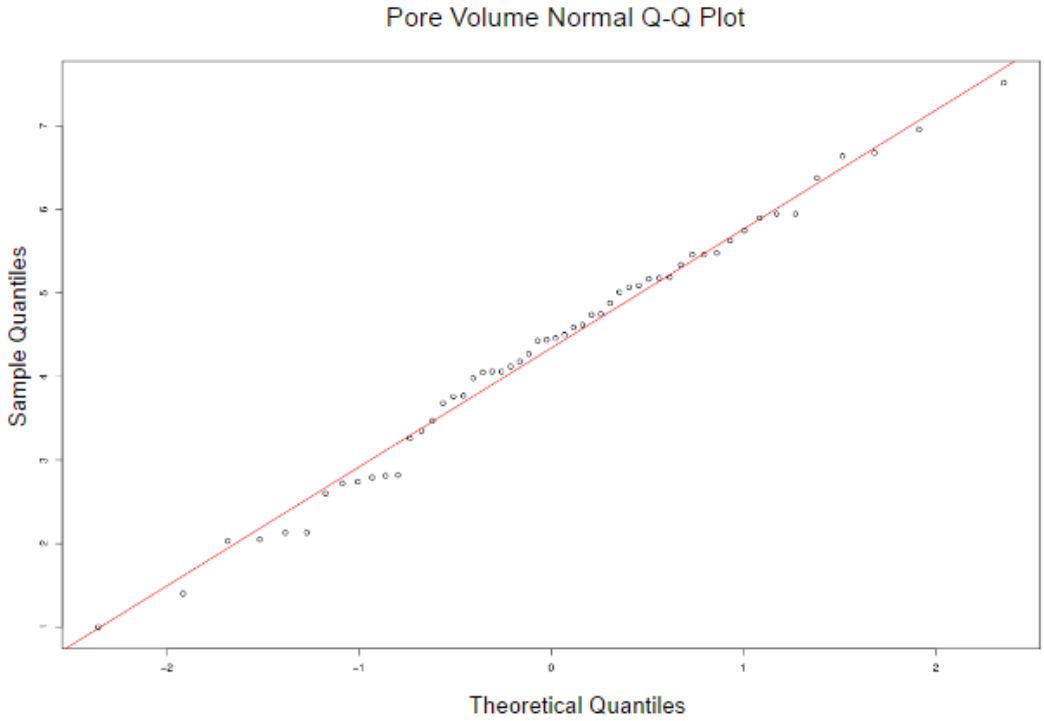

Figure 8 (above). A Q-Q plot of the distribution of pore volumes. Though the Q-Q plot seems to indicate normality, note the anomalies at theoretical quantiles -2 to -1.25, and consider the shape of the histogram. We conclude that the distribution of pore volumes is most likely nonnormal.

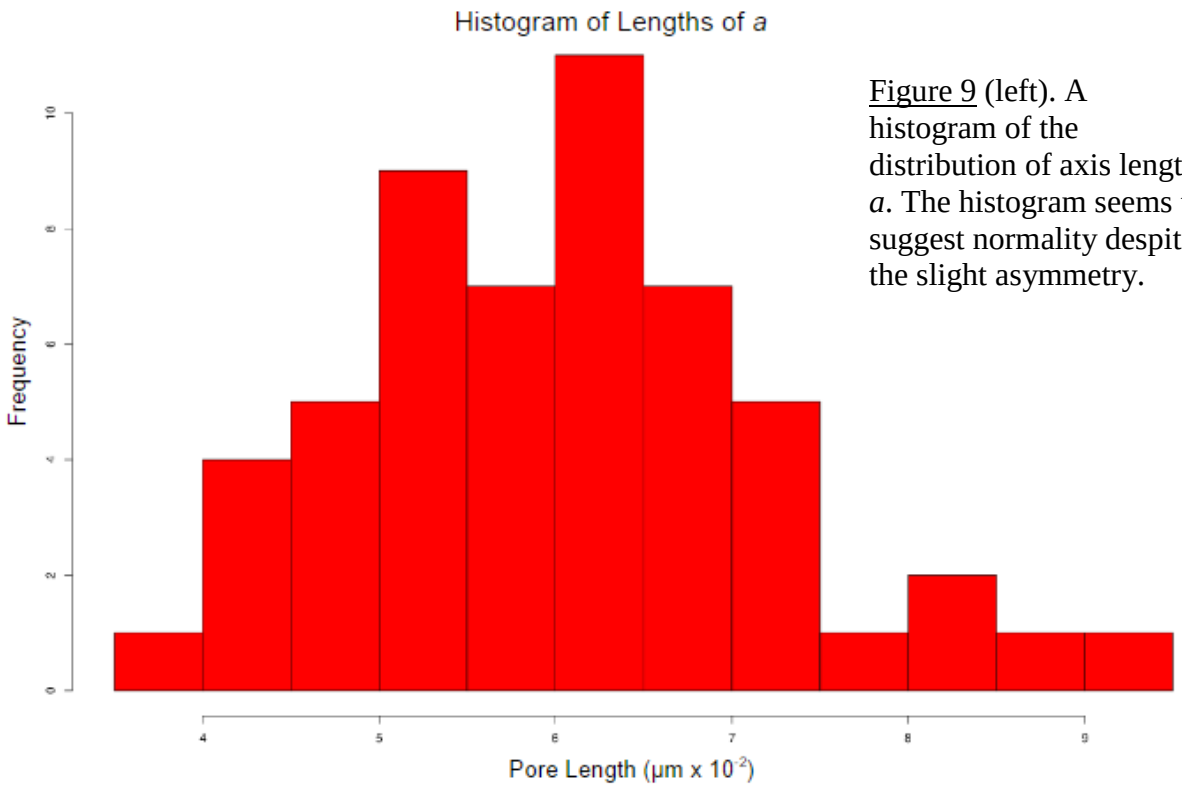

Figure 9 (left). A histogram of the distribution of axis length *a*. The histogram seems to suggest normality despite the slight asymmetry.

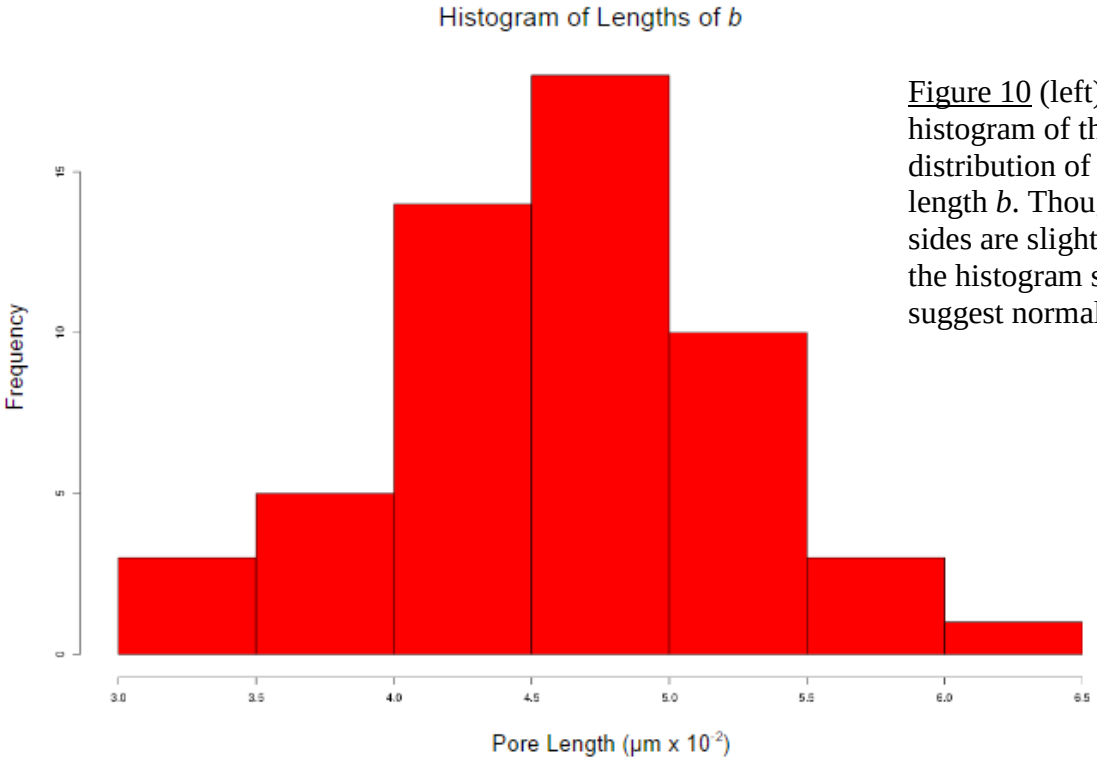

Figure 10 (left). A histogram of the distribution of axis length *b*. Though the sides are slightly uneven the histogram seems to suggest normality.

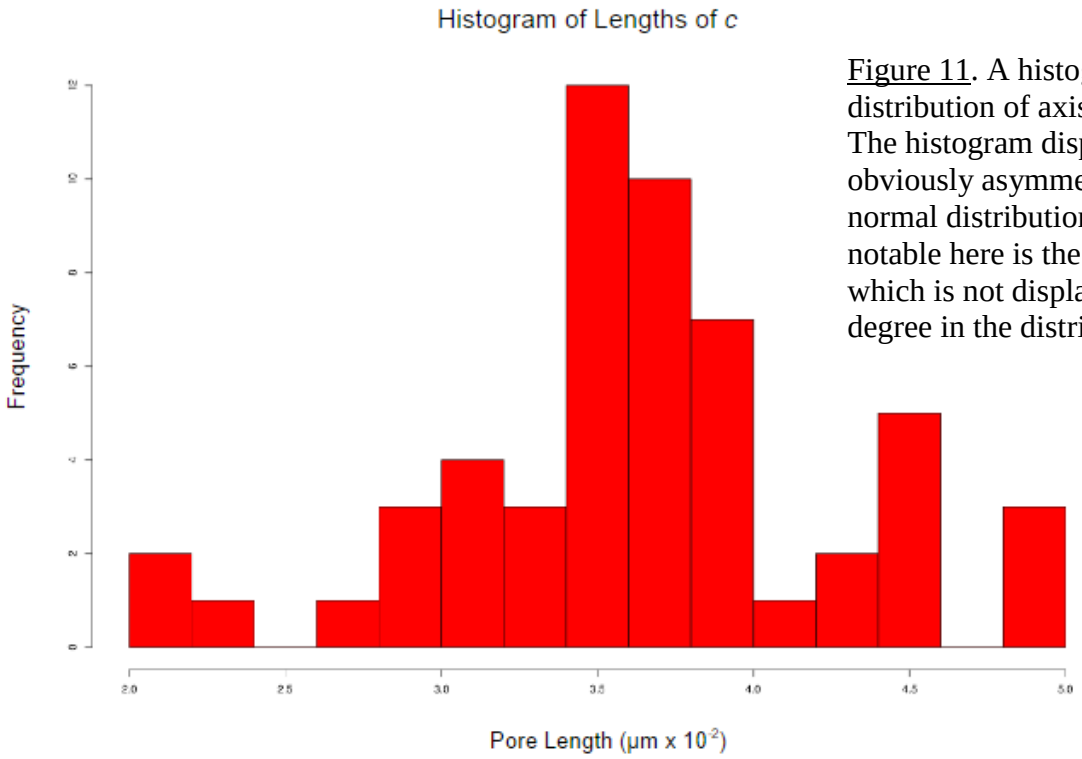

Figure 11. A histogram of the distribution of axis length *c*. The histogram displays an obviously asymmetrical, non-normal distribution. What is notable here is the large spread, which is not displayed to this degree in the distributions of *a*

Discussion:

Overview

By applying a novel technique of confocal microscopy to the investigation of porosity, we were able to effectively map out a three-dimensional structure of the pores in agarose hydrogel. Whereas significant and sudden changes in the position of the particle would indicate that the program was simultaneously tracking two or more different particles in the same data run, no such pattern was observed in the data we analyzed; indeed, all of the analyzed data displayed tracked particles with a suitable range of movements in the x, y, and z-axes. Moreover, as Figure 2 exemplifies, the intensity of light recorded in our data was both stable and high, indicating that the microscope was indeed tracking a fluorescent particle (rather than auto-fluorescing debris).

Comparison to Past Studies

Our findings differ slightly from those from previously published papers. One paper that took two-dimensional images of the cross-sections of pores asserted that the pores were roughly circular [7]; although this may be the case for some of the *cross-sections* of pores, we determined that the three-dimensional structure of pores was instead better described as *ellipsoidal*. Furthermore, the same study found that the distribution of the pore lengths displayed normality; yet as can be clearly seen by the histograms of *a*, *b*, and *c* (Figures 9-11), only two of the three distributions of the ellipsoidal axes displayed normality; moreover, whether the distribution of volume is normal remains questionable (given the contradiction between its Q-Q plot and its histogram in Figures 7 and 8, respectively).

A 1997 study found that the concentration of agarose hydrogel and average pore size are related by a power regression of $y = 573.5898 \cdot x^{-0.6366}$ (where y is the average pore diameter in nanometers and x is the concentration of agarose in the solution) [7]. Plugging in the agarose concentration of 2.6%, the power regression estimates the pores to be 312.19786 nm. However, if we convert the findings from our data to nanometers and double the lengths of *a*, *b*, and *c* to span the entire length of the ellipsoid in the x, y, and z directions, we receive 121.288 nm, 91.696 nm, and 72.680 nm. As is clearly evident, our results present pore sizes that are far smaller than those predicted by the paper's estimations.

Confocal Microscopy versus Atomic Force Microscopy

Confocal microscopy offers many distinct advantages over the traditional atomic force microscopy (AFM) that further enhances our understanding of the diffusion of macromolecules. It allows us to control the depth of the field of view as the particle moved through the pore. Fluorescence emission is filtered through a confocal pinhole to eliminate light from images

removed from the focal plane. The elimination of ambient light makes fluorescent particles easier to detect, and the tracking algorithm more accurate [13].

While AFM is strong in providing spatial sensitivity, among the surface of the sample, it inherently is lackluster at providing chemical sensitivity of the direct structural arrangement. Confocal microscopy provides both the spatial sensitivity and chemical sensitivity needed to observe the inherent structure [14]. The scanning is often slower, but it offers increased flexibility in acquiring images, especially relating to the size and depth. Through laser scanning confocal microscopy (LSCM), we were able to excise a thin optical slice of the original sample, with a physical thickness up to 100 μm precision, with suitable conditions allowing up to 500 nm precision. The AFM has a maximum depth of the range of 10,000 nm to 20,000 nm precision [15]. Thus, the method provides a reliable way to measure the true size of the pore in three-dimensional space, because a larger area of the surface of the sample is covered, compared to the approximate, local results obtained by AFM and even Field Emission Scanning Electron Microscope (FESFM) [15]. It is worth noting that while the AFM provides direct two-dimensional images of the surface of the sample [14], our single particle tracking method provides a three-dimensional plot of the particle's movement, and by association, the internal structure of the hydrogel.

Because the microscope used for AFM contacts the sample, the agarose may be disturbed, which may lead to a warping of the internal structure. Furthermore, to image the inside of the agarose with AFM, the hydrogel must be opened up, which could further affect the results derived from AFM [8].

Confocal Microscopy versus Diffusion of Macromolecules

Confocal microscopy further offers advantages in investigating porosity over a different method that we refer to as diffusion of macromolecules, which involves calculating the diffusion coefficient and deriving the pore size from a set of theoretical equations or models. For example, one commonly used method relies on the Ogston model, which assumes that pores are spherical, to calculate the diffusion coefficient using fiber radius and specific fiber length, amongst other parameters [16]. Another model, called the reptation model, may rely on parameters such as the DNA electric charge and free space to calculate the diffusion constant.

However, as we have shown, many pores are better described as ellipsoidal. Because our method does not rely on the previous theoretical equations, the accuracy of our approximation of the pore size is not affected by the pore's ellipsoidal shape (as it would be with the Ogston model). More importantly, several of the aforementioned parameters (such as fiber radius, free space, and DNA electric charge) are difficult to accurately calculate; therefore, a not-inconsequential amount of error may be expected with a method that calculates diffusion coefficients using theoretical models. We do not rely on parameters with a large degree of error; nor do we assume that our pores fit their theoretical definition (for example, having a spherical structure). Confocal microscopy, thus, provides more conclusive results for the size and structural arrangement of pores.

Conclusions and Future Work:

On a set of 54 data runs, our data indicates that for an ellipsoidal approximation, the average a, b, and c values for the semi-principal axes are 6.0644×10^{-2} μm, 4.5848×10^{-2} μm, and 3.6340×10^{-2} μm with a standard deviation of 1.1745×10^{-2}, 6.6169×10^{-3}, and 6.1717×10^{-2} respectively. The smallest volume of a single pore was 1×10^{-4} μm^3 and the largest was 7.52 x

10^{-4} μm^3. The mean volume of the pores was 4.3417 x 10^{-4} μm^3, with a standard deviation of 1.4558 x 10^{-4}.

To our knowledge, before our study, no research on the porosity of agarose hydrogel had been done utilizing the promising technology of single fluorescent particle tracking to the study of agarose hydrogel. Such a method is extremely unlikely to damage the internal structure of the agarose, as opposed to other methods that might warp the arrangement of the pores. As one of the first of its kind to accumulate a large amount of data using a single particle tracking method, our research project investigates agarose hydrogel from a perspective that has yet to be fully explored by modern science. Our method does not rely on theoretical assumptions about the shape of the pore, nor does it use parameters like fiber radius that are not easily accurately calculated. Moreover, single particle tracking does not affect the internal structure of the agarose in the same way that a microscope contacting the agarose might warp the sample.

Had we more time, we would have developed a method to automate the identification and approximation of pores. We manually selected and excised the pores to be analysis; while this allows for personal confirmation that a potential pore is indeed one pore, rather than a cluster of several pores, it can also be inefficient at times. One potential method that we considered but did not explore involved recognizing when the axes of an ellipsoidal approximation suddenly change dramatically, in either direction or length, thereby indicating that the particle has left the pore. Further experiments that utilize water as a medium as opposed to glycerol may be performed to confirm our results, as water is conventionally the medium in which agarose hydrogel is used in biomedical applications. Another question that might be answered would be whether the relative arrangement of pores follows any regular pattern. If so, our understanding of the internal structure of the hydrogel would greatly benefit.

On the whole, our project has produced valuable insight into the porosity of agarose hydrogel. We have calculated a rough estimate of the volume of a pore in agarose hydrogel, ranging from 1×10^{-4} μm^3 to 6.68×10^{-4} μm^3 with an average of 4.338×10^{-4} μm^3. Consequently, we have also demonstrated that the pores in agarose hydrogel are roughly shaped like an ellipsoid, with many pores more closely resembling spheres. It is important to note that our project is one of the first to apply single particle tracking using a confocal microscope to the study of the porosity of agarose hydrogel. As such, our research project paves the way for future investigations of the substance that is ubiquitous across the biotechnology field, yet not sufficiently studied. Once our understanding of agarose hydrogel is complete, its possibilities as an important component of biomedical applications become limitless.

References:

[1] Narayanan, J.; Xiong, J.-Y.; Liu, X.-Y. Determination of Agarose Gel Pore Size: Absorbance Measurements Vis a Vis Other Techniques. *J. Phys.: Conf. Ser. Journal of Physics: Conference Series* **2006**, *28*, 83–86.

[2] Wang, N., & Wu, X. S. (1997). Preparation and Characterization of Agarose Hydrogel Nanoparticles for Protein and Peptide Drug Delivery. *Pharmaceutical Development and Technology, 2*(2), 135-142. doi:10.3109/10837459709022618

[3] Varoni, E., Tschon, M., Palazzo, B., Nitti, P., Martini, L., & Rimondini, L. (2012). Agarose Gel as Biomaterial or Scaffold for Implantation Surgery: Characterization, Histological and Histomorphometric Study on Soft Tissue Response. *Connective Tissue Research, 53*(6), 548-554. doi:10.3109/03008207.2012.712583

[4] Zhu, J., & Marchant, R. E. (2011). Design properties of hydrogel tissue-engineering scaffolds. *Expert Review of Medical Devices, 8*(5), 607-626. doi:10.1586/erd.11.27

[5] Ahmed, E. M. (2015, March). Hydrogel: Preparation, characterization, and applications: A review. *Journal of Advanced Research, 6*(2), 101-121. Retrieved September 19, 2016, from http://www.sciencedirect.com/science/article/pii/S2090123213000969

[6] Trappmann, B., Gautrot, J. E., Connelly, J. T., Strange, D. G., Li, Y., Oyen, M. L., . . . Huck, W. T. (2012). Extracellular-matrix tethering regulates stem-cell fate. *Nature Materials Nat Mater, 11*(7), 642-649. doi:10.1038/nmat3339

[7] Pluen, A., Netti, P. A., Jain, R. K., & Berk, D. A. (1999). Diffusion of Macromolecules in Agarose Gels: Comparison of Linear and Globular Configurations. *Biophysical Journal, 77*(1), 542-552. doi:10.1016/s0006-3495(99)76911-0

[8] Pernodet, N., Maaloum, M., & Tinland, B. (1997). Pore size of agarose gels by atomic force microscopy. *Electrophoresis, 18*(1), 55-58. doi:10.1002/elps.1150180111

[9] Ashley, T. T., Competition Entrant, Competition Entrant, & Andersson, S. B. (2016). Tracking single fluorescent particles in three dimensions via extremum seeking. *Biomedical Optics Express Biomed. Opt. Express, 7*(9), 3355. doi:10.1364/boe.7.003355

[10] Raschka, S. (2014, April 13). Implementing a Principal Component Analysis (PCA). Retrieved September 20, 2016, from http://sebastianraschka.com/Articles/2014_pca_step_by_step.html

[11] Miller, C. C. (1924, December 01). The Stokes-Einstein Law for Diffusion in Solution. *Proceedings of the Royal Society A: Mathematical, Physical and Engineering Sciences, 106*(740), 724-749. doi:10.1098/rspa.1924.0100

[12] Cappe, O. (2009, August 31). Online sequential Monte Carlo EM algorithm. *2009 IEEE/SP 15th Workshop on Statistical Signal Processing,* 37-40. doi:10.1109/ssp.2009.5278646

[13] Webb, R. H. (1996). Confocal Scanning Optical Microscopy and Related Imaging Systems. *Reports on Progress in Physics, 59*, 427-471. doi:10.1016/b978-0-12-408750-7.x5008-3

[14] Eftaiha, A. F., Brunet, S. M., Paige, M. F., & Mendez-Vilas, A. (n.d.). A comparison of atomic force microscopy, confocal fluorescence microscopy and brewster angle microscopy for characterizing mixed monolayer surfactant films. In *In Current Microscopy Contributions to Advances in Science and Technology* (pp. 1438-1447). Spain: Formatex Research Center.

[15] Oyarzún, D. P., Pérez, O. E., Teijelo, M. L., Zúñiga, C., Jeraldo, E., Geraldo, D. A., & Arratia-Perez, R. (2016, November). Atomic force microscopy (AFM) and 3D confocal microscopy as alternative techniques for the morphological characterization of anodic TiO2 nanoporous layers. *Materials Letters, 165*, 67-70. doi:10.1016/j.matlet.2015.11.087

[16] Labrie, J., Mercier, J., & Slater, G. W. (2000, March 01). An exactly solvable Ogston model of gel electrophoresis. Attractive gel-analyte interactions and their effects on the Ferguson plot. *Electrophoresis, 21*(5), 823-833. doi:10.1002/(sici)1522-2683(20000301)21:53.0.co;2-4